

Superfluid transition of ^4He films adsorbed in porous materials

Vincent Kotsubo* and Gary A. Williams

Physics Department, University of California, Los Angeles, California 90024

(Received 21 October 1985)

The superfluid transition of thin ^4He films adsorbed in Al_2O_3 packed powders is studied using third-sound techniques. For powder grain sizes down to 500 Å, the transition is found to remain a Kosterlitz-Thouless vortex-screening transition. As the powder size is decreased, however, the drop to zero of the areal superfluid density becomes broadened, and the third-sound attenuation decreases. A finite-size model of the Kosterlitz-Thouless transition is formulated to explain these effects. Limiting the maximum vortex pair separation to the powder grain size leads to a broadening of the transition and reduced dissipation if the grain size is smaller than a vortex diffusion length. The model also describes many features of earlier measurements on films adsorbed in porous Vycor glass. The claim that the transition in Vycor films is three dimensional (not involving vortices) is reexamined in light of the present results.

I. INTRODUCTION

The superfluid transition in ^4He has long been a testing ground for theories of statistical mechanics. Onsager¹ and Feynman² first recognized that the superfluid wave function has two components, a magnitude and a phase. The two-component order parameter puts helium in the same universality class as the extensively studied XY model of magnetism. A recurring question in these systems has been the role of topological excitations in the phase transition that destroys the ordered state. Onsager and Feynman showed that quantized vortices were the low-energy topological excitations in helium, and both proposed in their initial papers^{1,2} that vortex lines and rings could be the cause of the superfluid λ transition. The Hamiltonian of the XY model similarly contains vortex eigenvalue solutions, but the vortex contribution to the phase transition has never been clearly demonstrated for three-dimensional (3D) systems, although there have been numerous attempts.³⁻⁵ High-temperature expansions of the 3D XY model,⁶ and later the ϵ expansion of the same model,⁷ have proven to be successful in calculating the critical exponents of the transition, and these have been well verified by experiments in helium at the λ point.⁸ However, these expansions are very formal and mathematical, and the effects of the vortex excitations cannot be followed through the complex calculations.⁹

It is only in two dimensions (2D) that the role of vortices has clearly been demonstrated. Kosterlitz and Thouless¹⁰ (KT) showed that by considering pairs of vortices with opposite circulation the properties of the phase transition in 2D helium films and in the 2D XY model could be calculated using simple arguments.¹¹ In this theory vortex pairs of a given separation are strongly screened by vortex pairs of smaller separation between them. The most famous prediction of the theory¹² is the universal "jump" to zero of the areal superfluid density at a critical onset temperature in helium films. (The equivalent quantity in the XY model is the helicity modulus.^{13,14}) This prediction has been verified for helium films adsorbed on

flat substrates, both in third-sound experiments¹⁵ and in Andronikashvili-type oscillator measurements.¹⁶⁻¹⁹

However, the nature of the superfluid transition for helium films adsorbed in porous materials is not so clear. In 1977 Reppy and co-workers²⁰⁻²² at Cornell University carried out torsion-oscillator measurements on films adsorbed in porous Vycor glass, and found rather different results from the flat-substrate case. They observed a broadened and continuous decrease of the superfluid mass to zero, rather than the abrupt jump seen on flat substrates. They also could not observe any excess dissipation at the transition, in contrast to the sharp peaks seen for flat-substrate films.¹⁷⁻¹⁹ Over a limited range near the transition, their measurements of the superfluid mass could be fitted with a power law, $m_s \sim (T_c - T)^\delta$, where averaging exponents of curves of different film thickness gave $\delta=0.63$. Since this is close to the bulk-liquid exponent 0.67,^{8,23} Reppy and co-workers proposed that the transition for films in Vycor is three dimensional, not involving vortices at all. In their most recent work^{24,25} they have claimed to observe a crossover to the dilute limit of this transition at very low temperatures, the dilute Bose gas.

It was this striking apparent change in the nature of the superfluid transition in ^4He films, between flat substrates and porous materials, which has motivated our experiments using packed-powder substrates. The question is at what powder grain size will the 2D vortex transition be superceded by the 3D transition? Clearly, for very large grain sizes the transition must be the same as found on flat substrates. As the grain size is reduced toward the 150-Å grain size of the Vycor, however, it seemed there must be a clear crossover between the 2D and 3D behavior at some length scale. The two types of phase transition involve completely different mechanisms, and hence we undertook detailed third-sound measurements at the superfluid onset point to try to detect this changeover between the two. We have employed three different powder diameters (1 μm , 3000 Å, and 500 Å) to try to span the range between flat substrates and the 150-Å Vycor.

In fact, we have observed no such crossover behavior. We find that the transition continues to occur at the 2D Kosterlitz-Thouless point even for the smallest, 500-Å, powder. As the grain size is reduced, however, there is a broadening of the transition, and a reduction of the third-sound attenuation. We attribute this to finite-size modifications of the KT transition, with the finite scale being set by the power grain size.

Brief reports of our experiments have been published previously,^{26–28} and in this paper we give a more complete account of the work. In Sec. II we formulate a model for the finite-size KT transition. In Sec. III we describe the experimental apparatus and procedure, and in Sec. IV we present the data and analysis. In Sec. V the Vycor data of Reppy and co-workers and the arguments leading to the 3D Bose transition hypothesis are reexamined. We propose an alternate hypothesis, namely that the Vycor data are, in fact, well described as a finite-size KT transition. In Sec. VI we discuss some of the implications of our results, and suggest further experiments that are needed to resolve these issues.

II. THEORY

A. Spherical model

The experiments are carried out with the helium film adsorbed on powder particles that are roughly spherical in shape. To model this situation we adapt the Kosterlitz-Thouless vortex-screening arguments to a spherical surface. The geometry needed for the calculation is shown in Fig. 1, where two vortices of opposite circulation are separated by a central angle θ on a sphere of radius R . The energy of this configuration can be calculated using the spherical coordinates (θ, ϕ) , with one vortex at $(0, 0)$ and the other at $(\theta, 0)$. The flow field at the point (θ', ϕ') from this configuration can be found from the analysis of Bogomolov,²⁹

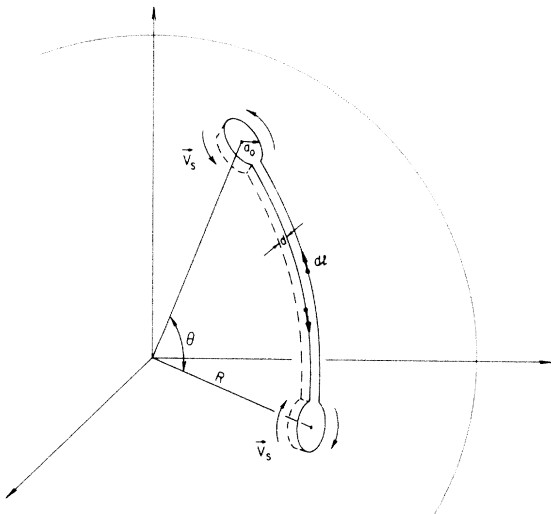


FIG. 1. Schematic of a vortex-antivortex pair on a sphere, showing the cut used in evaluating Eq. (2).

$$v_{s\theta} = \frac{1}{2R} \frac{\hbar}{m} \left[\frac{\sin\theta \sin\phi'}{1 - \sin\theta \sin\theta' \cos\phi' - \cos\theta \cos\theta'} \right], \quad (1)$$

$$v_{s\phi} = \frac{1}{2R} \frac{\hbar}{m} \left[\frac{\sin\theta'}{1 - \cos\theta'} + \frac{\sin\theta \cos\theta' \cos\phi' - \cos\theta \sin\theta'}{1 - \sin\theta \sin\theta' \cos\phi' - \cos\theta \cos\theta'} \right],$$

where m is the helium atomic mass. The energy (in units of $k_B T$) is given by

$$U_0 = \frac{1}{k_B T} \int \frac{1}{2} \rho_s^0 v_s^2 dV + 2E_c, \quad (2)$$

where the integration over the volume of the film excludes the vortex-core regions of radius a_0 , and the energies of the vortex cores are included as the additive term $2E_c$. ρ_s^0 is the volume superfluid density and, in general, will vary across the thickness of the film. The integration of Eq. (2) is most easily carried out by converting the volume integral to a surface integral,³⁰ with the surface including a cut in the film along the arc connecting the two vortices, shown in Fig. 1. The cut is closed by circular paths of radius a_0 about each core. We neglect the contributions from the circular paths: this is exact if the cores are circular,³⁰ but corrections may be necessary depending on the degree of distortion of the cores.³¹ The result of this calculation gives, for the vortex pair energy,

$$U_0(\theta) = 2\pi K_0 \ln \left[\frac{\sin[\frac{1}{2}(\theta - \theta_c)]}{\sin(\frac{1}{2}\theta_c)} \right] + 2E_c, \quad (3)$$

where $\theta_c = a_0/R$ and $K_0 = (\hbar/m)^2 (\sigma_s^0/k_B T)$. σ_s^0 is the areal superfluid density and is given by $\sigma_s^0 = \langle \rho_s^0 \rangle d$, where ρ_s^0 is averaged over the film of thickness d . In the limit of small θ , U_0 reduces to the flat-substrate form $2\pi K_0 \ln[(r - a_0)/a_0]$, where r is the separation of the vortex centers.³² The result for U_0 is easily checked for the case $\theta = \pi$, where the v_s of Eq. (1) becomes simple and the integral in Eq. (2) can be carried out directly; the result is exactly that of Eq. (3) with $\theta = \pi$.

In an external flow field the vortex pairs are polarized and act to screen the field. The polarizability $P(\theta)$ is computed following Kosterlitz and Thouless,¹⁰

$$P(\theta) = \frac{1}{2} \frac{\hbar}{m} \frac{\partial}{\partial v_{\text{ext}}} \langle R \theta \cos\psi \rangle \Big|_{v_{\text{ext}}=0}, \quad (4)$$

where ψ is the angle between the flow v_{ext} and the arc joining the centers of the vortices. The average is weighted by the Boltzmann factor

$$\exp \left[-U_0(\theta) - 2\pi K_0 \frac{m}{\hbar} v_{\text{ext}} R \theta \cos\psi \right]. \quad (5)$$

Carrying out the average by first taking the derivative with respect to v_{ext} , taking the limit $v_{\text{ext}} \rightarrow 0$, and then integrating gives the result

$$P(\theta) = \pi K_0 \frac{(R\theta)^2}{2}. \quad (6)$$

The above result assumes that the vortex-antivortex-pair separation is small so that the velocity of the external flow field is constant over the extent of the dipole pair. This assumption will no longer be valid for pairs with separation on the order of the sphere size. However, pairs of this size will only be significant at high temperatures where the superfluid density approaches zero. In this regime there is a second factor which also makes the calculation inaccurate: the vortex density becomes high, and the KT assumption of a dilute gas of vortices is no longer a good approximation.

The behavior of the superfluid density in the region of the transition is determined by the screening effects of the vortex-antivortex pairs. This screening lowers the observable superfluid density σ_s , and is described using a "dielectric constant":

$$\sigma_s = \frac{\sigma_s^0}{\epsilon(\theta)}, \quad (7)$$

where σ_s^0 is the superfluid density in the absence of vortices. The dielectric constant is length dependent, since the behavior of a particular pair depends on the screening due to smaller pairs.¹⁰ The dielectric constant can be written as $\epsilon(\theta) = 1 + 4\pi\chi(\theta)$, where the susceptibility $\chi(\theta)$ is

$$\chi(\theta) = \int_{2\theta_c}^{\theta} n(\theta')P(\theta')2\pi R^2 \sin\theta' d\theta'. \quad (8)$$

The integration starts from $2\theta_c = 2(a_0/R)$, and corresponds to the point where the two vortex cores are in contact and $U_0(\theta) = 2E_c$. $P(\theta)$ is the polarizability of a pair derived above, while $n(\theta)$ is the density of pairs with angular separation θ and is the Boltzmann factor multiplied by the phase space:

$$n(\theta) = \frac{y_0^2}{(2R\theta_c)^4} e^{-U(\theta)}, \quad (9)$$

where $y_0 = \exp(-E_c)$ and $U(\theta)$ is the energy of interaction of a vortex-antivortex pair, including the effects of screening. This energy is determined by integrating the force between the vortices:

$$U(\theta) = \int_{2\theta_c}^{\theta} \frac{1}{\epsilon(\theta')} \frac{dU_0}{d\theta'} d\theta', \quad (10)$$

where U_0 is the energy of an isolated vortex-antivortex pair derived above. Making the substitution $K(\theta) = (\hbar/m)^2(\sigma_s/k_B T)$, Eqs. (7)–(10) become

$$\frac{1}{K(\theta)} = \frac{1}{K_0} + \frac{4\pi^3 y_0^2}{(2\theta_c)^4} \int_{2\theta_c}^{\theta} (\theta')^2 \sin\theta' e^{-U(\theta')} d\theta', \quad (11)$$

with

$$U(\theta') = \int_{2\theta_c}^{\theta'} \frac{\pi K(\theta'')}{\tan[\frac{1}{2}(\theta'' - \theta_c)]} d\theta''. \quad (12)$$

These integral equations are the main result of the modified KT theory for a sphere, giving the renormalized $K(\theta)$ in terms of the "bare" parameters y_0 and K_0 . In the limit of large R (i.e., θ small), these equations reduce to flat-substrate results

$$\frac{1}{K(r)} = \frac{1}{K_0} + 4\pi^3 \frac{y_0^2}{(2a_0)^4} \int_{2a_0}^r (r')^3 e^{-U(r')} dr', \quad (13)$$

$$U(r) = \int_{2a_0}^r \frac{\pi K dr'}{r' - a_0}. \quad (14)$$

These are nearly the same as the equations given by Young,¹¹ the only differences arise from the use of $\ln[(r - a_0)/a_0]$ rather than $\ln(r/a_0)$ in the interaction potential.

Equation (11) can be solved by iteration, starting with the unscreened value $K = K_0$ at $\theta = 2\theta_c$ and integrating over the sphere to $\theta = \pi$. The resulting values of K as a function of K_0 are shown in Fig. 2, for several different sphere sizes. In the flat-substrate case ($R \rightarrow \infty$) the dotted-dashed line shows the abrupt drop to zero of the superfluid density at the critical value $K = 2/\pi$. This corresponds to the famous "universal jump" of the KT theory, where the critical value of σ_s occurs at the temperature T_c given by the relation¹²

$$\frac{\sigma_s}{T_c} = \frac{2}{\pi} \left[\frac{m}{\hbar} \right]^2 k_B = 3.5 \times 10^{-9} \text{ g/cm}^2 \text{ K}. \quad (15)$$

For finite sphere sizes, however, the drop in σ_s is not abrupt. With decreasing R/a_0 the transition becomes more broadened and spread out. Figure 3 shows the K -versus- K_0 curves of Fig. 2 converted to plots of σ_s versus T for the particular choice $\sigma_s^0 = 5.0 \times 10^{-9} \text{ g/cm}^2$. The broadening of the transition results from the fact that the iteration of Eq. (11) is no longer carried out to infinite vortex separation, as in the flat-substrate case, but is cut off at the maximum separation of half the sphere circumference, πR . This leads to a finite-size rounding of the KT "jump" in σ_s . Figure 4 shows σ_s as a function of both temperature and film thickness; the upper curves are the $R \rightarrow \infty$ flat-substrate case, while the lower curves are for the 150-Å sphere. In both plots the straight solid line has the slope given by Eq. (15) and marks the onset point of the KT jump.

A prominent feature of the smaller sphere sizes in Figs. 2–4 is the "tail" region of the transition where the curva-

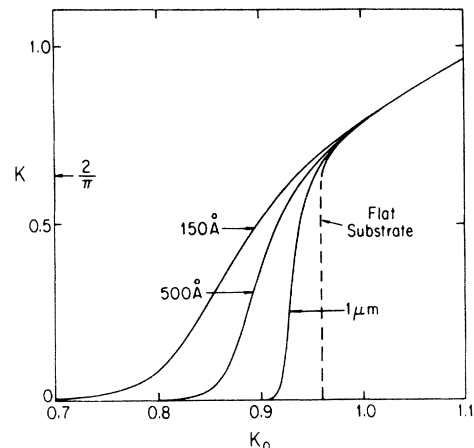


FIG. 2. Renormalized K as a function of K_0 , for different sphere diameters. The parameters used in the calculation are $E_c/K_0 = 2.2$ and $a_0 = 10 \text{ \AA}$.

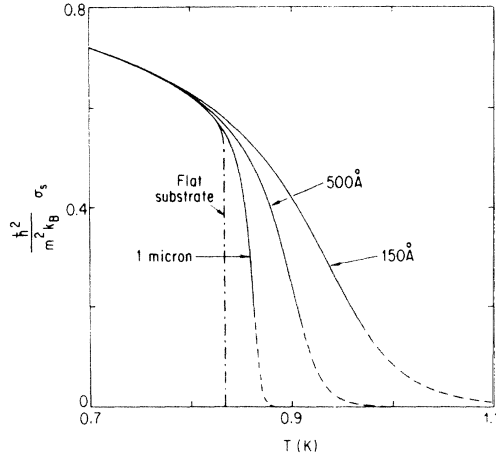


FIG. 3. Areal superfluid density vs temperature, obtained from the curves in Fig. 2 for the choice $\sigma_s^0 = 5.0 \times 10^{-9}$ g/cm 2 . The dashed lines show the regions where $y > y_0$. The dotted-dashed line shows the universal KT “jump” in the flat-substrate limit $R \rightarrow \infty$.

ture of σ_s changes sign as it becomes small. This is a consequence of the finite-size restriction of the model. As is well known, a finite system cannot have a true thermodynamic phase transition with a sharply defined critical temperature. The superfluid density in Figs. 2–4 becomes very small in the tail region, but there is no tem-

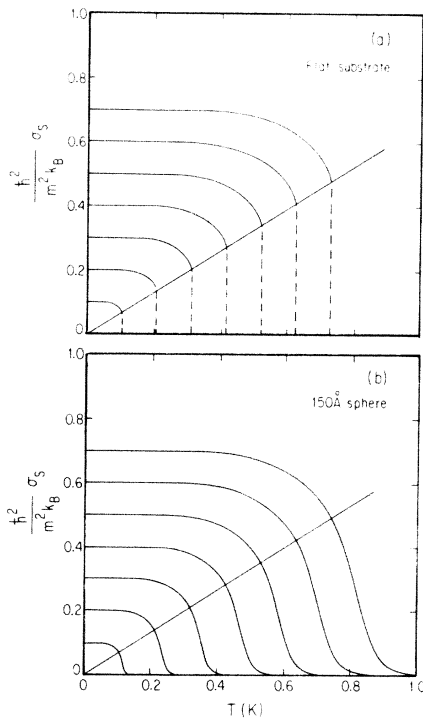


FIG. 4. Areal superfluid density versus temperature for different film thicknesses using the curves from Fig. 2. The film thickness is parametrized by different values of σ_s^0 ($\sigma_s^0 = \sigma_s$ at $T=0$), and σ_s^0 is taken to be temperature independent below 1 K. (a) The upper curves are for the flat-substrate case, and (b) the lower curves are for a 150-Å diameter sphere. The straight line in both figures has the slope given by Eq. (15) and marks the KT onset point.

perature at which it becomes identically zero (except, of course, for the case that the “background” $\sigma_s^0 = 0$).

In Fig. 3 the dashed portions of the curves in the tail region show where the vortex fugacity

$$y = y_0 \left[\frac{\theta^3 \sin \theta e^{-U(\theta)}}{(2\theta_c)^4} \right]^{1/2} \quad (16)$$

exceeds the initial value y_0 at some value of θ in the iteration. In these regions the vortex density is becoming high enough that the dilute dipole-gas approximation is beginning to break down. Quadrupole and higher-order terms will become appreciable and act to further screen the superfluid density. We have not attempted to include such effects in our model since the calculations become quite complicated,³³ but qualitatively the screening would tend to further lower σ_s in the dashed regions and reduce the size of the tail.

The broadening of the KT transition for finite-size systems has also been observed in Monte Carlo simulations of the 2D XY model.^{14,34} The parameter corresponding to the superfluid density in the XY model is the helicity modulus, the response of the spins to an applied phase twist.¹³ For large lattices the modulus drops rapidly to zero at the critical KT point, but as the lattice size is decreased¹⁴ the drop becomes much slower and broadened out in temperature, quite similar to our Fig. 3. The “tail” region is clearly observed in these simulations: there is a change in the sign of the curvature of the modulus as it falls to zero, and its derivative approaches zero.

The concept of a finite-size KT transition has recently been applied to two other physical systems. Fiory *et al.*³⁵ have studied the KT transition in granular superconducting films. They use a finite-length cutoff of the KT recursion relations to explain a broadening of the jump in density of superconducting electrons at the transition. A finite-size KT analysis has also been used recently to describe two-dimensional magnetic materials in intercalated graphite.³⁶ The susceptibility of the 2D XY model is calculated by terminating the recursion relations at a finite scale, the size of the intercalant islands. This leads to a broadening of the susceptibility drop at the transition, in agreement with the experiments.³⁷

B. Finite-frequency effects

The above theoretical model is valid only for the static limit of zero frequency. To facilitate comparison with finite-frequency experiments it is necessary to take into account the diffusive motion of the vortices. This has been worked out for the flat-substrate case by Ambegaokar, Halperin, Nelson, and Siggia³⁸ (AHNS). The main parameter in this theory is the diffusion length $r_D = \sqrt{2D/\omega}$, where D is the diffusion constant of a vortex and ω is the angular frequency. Vortices of separation $r < r_D$ are able to follow the oscillating drive field, while those with separation greater than r_D cannot respond to the drive. This leads to a broadening of the KT transition, since the iteration of Eq. (13) must now be cut off at the length r_D rather than extending to infinity. It also

leads to appreciable dissipation in the vicinity of the transition, arising from the diffusive motion of vortex pairs of separation near r_D , which are maximally out of phase with the drive. This finite-size broadening of the transition and the accompanying dissipation peak have been observed in the flat-substrate experiments of Reppy and co-workers.¹⁷⁻¹⁹

The finite-frequency calculation can be extended to our spherical KT model. Following AHNS, the dielectric constant becomes frequency dependent,

$$\epsilon(\theta, \omega) = 1 + \int_{2\theta_c}^{\theta} \frac{d\hat{\epsilon}}{\partial\theta} g(\theta, \omega) d\theta, \quad (17)$$

where $\hat{\epsilon}$ is the static dielectric constant and $g(\theta, \omega)$ is the vortex response function, which satisfies the Fokker-Planck equation describing the diffusive motion. For the spherical geometry Wang and Yu³⁹ find $g(\theta, \omega)$ to be given by

$$g(\theta, \omega) = \frac{1}{1 - i(R/r_D)^2 f^{-1}(\theta)}, \quad (18)$$

where

$$f(\theta) = \frac{1}{\theta} \left[\frac{\pi K(\theta)}{\tan[\frac{1}{2}(\theta - \theta_c)]} - \cot(\theta) \right]. \quad (19)$$

It can be seen from Eq. (18) that the important scale factor for the spherical case is $(R/r_D)^2$. For R appreciably larger than r_D , Eq. (18) becomes equivalent to the flat-substrate result, and the broadening and attenuation are independent of R and are controlled only by r_D . For R smaller than r_D , however, the imaginary term in Eq. (18) becomes small. The vortex separation will always be less than r_D in this case, and the attenuation arising from the imaginary part of $g(\theta, \omega)$ will decrease as $(R/r_D)^2$. The broadening of the transition in the limit $R \ll r_D$ is determined only by the finite sphere size, and is identical to the static superfluid density determined by Eq. (11).

Figure 5 shows the result of calculating the frequency-dependent dielectric constant for several sphere sizes using Eqs. (17)–(19). The dissipation is displayed in terms of the change in quality factor Q of a torsion oscillator,

$$\Delta(1/Q) = (A/M)\sigma_s^0 \text{Im}(1/\epsilon). \quad (20)$$

Here, A/M is the ratio of the surface area to the mass of the substrate and the value used, $2.7 \times 10^3 \text{ cm}^2/\text{g}$, is similar to that found in the oscillators used in experiments.^{17,19} A background dissipation of $1/Q_{\text{back}} = 1 \times 10^{-10}$ is added to the calculated dissipation in order that a logarithmic plot can be used to display the large variations in magnitude. The plotted $1/Q$ is then $1/Q = 1/Q_{\text{back}} + \Delta(1/Q)$. For the diffusion constant an intermediate value $D/a_0^2 = 2.5 \times 10^{10} \text{ sec}^{-1}$ has been chosen.⁴⁰ Previous experimental estimates have ranged from 10^8 to 10^{11} sec^{-1} in thermal-conductivity measurements,⁴¹ and from 10^{11} to 10^{16} sec^{-1} in the torsion-oscillator experiments.^{17,19}

The most striking result of these calculations is how substantially the dissipation is reduced as the sphere size is reduced. The peak dissipation for the 500-Å sphere size is down by about 3 orders of magnitude as compared with

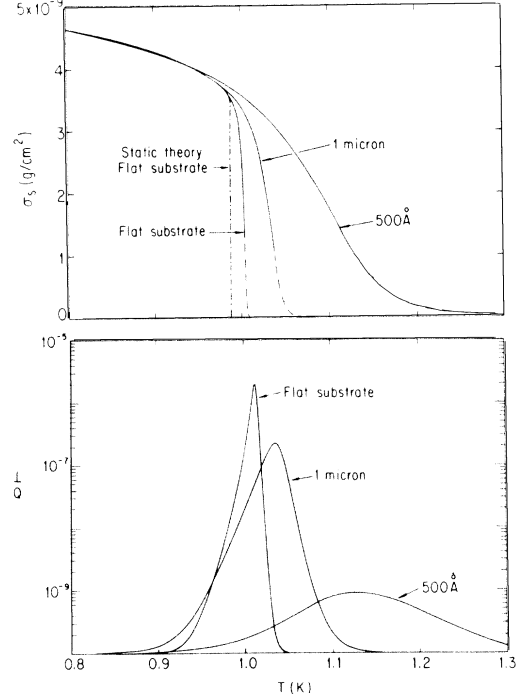


FIG. 5. Finite-frequency calculations of the areal superfluid density (top) and dissipation (bottom), assuming torsion-oscillator parameters. The dashed curves show where $y > y_0$, and the dotted-dashed line shows the $\omega=0$ flat-substrate result. The parameters used are $E_c/K_0=2.2$, $a_0=20 \text{ \AA}$, $D/a_0^2=2.5 \times 10^{10} \text{ sec}^{-1}$, $\omega=8.3 \times 10^3 \text{ rad/sec}$, $A/M=2.7 \times 10^3 \text{ cm}^2/\text{g}$, $1/Q_{\text{back}}=1 \times 10^{-10}$, and $\sigma_s^0=5.0 \times 10^{-9} \text{ g/cm}^2$.

the flat substrate, and drops roughly as the ratio $(R/r_D)^2$. The broadening of σ_s for the 500-Å sphere is entirely due to the sphere size and is frequency independent. The 1- μm σ_s curve shows some additional broadening at finite frequencies, since it is closer to the diffusion length of $r_D \sim 3 \mu\text{m}$ used in Fig. 5.

We have not included the “free”-vortex contribution in these calculations since it is not evident how to apply it to the sphere model. In the AHNS calculation this concept was introduced to circumvent difficulties with the Kosterlitz-Thouless recursion relations in the region of high vortex densities. The same difficulties are also present in our model, and so the results for dissipation should not strictly apply in the region where the superfluid density is close to zero. It is not clear what effect the inclusion of the free-vortex contribution would have on our calculations. Even for the flat-substrate case, detailed data analysis by Agnolet¹⁹ did not clearly determine the extent of the free-vortex contribution.

C. Third sound

In the experiments to be described in the next section, the velocity and attenuation of third sound are the measured quantities. Third sound is a thickness (and temperature) wave in the film, where the van der Waals force is the restoring force that determines the wave velocity.⁴² For a film on a flat substrate, and in the absence of vor-

tices, the velocity can be written as

$$c_{30}^2 = \frac{\sigma_s^0}{\rho} \frac{3\alpha}{d^4}, \quad (21)$$

where α is the van der Waals coefficient and d is the total thickness of the helium film. Rudnick and co-workers⁴³ have shown that σ_s^0 is related to the film thickness by the phenomenological relation

$$\sigma_s^0 = \rho_s^b (d - D_0), \quad (22)$$

where ρ_s^b is the temperature-dependent bulk superfluid density and D_0 is an effective length that accounts for the nonsuperfluid part of the film (the solid layer, healing effects, etc.).

In the presence of vortices Eq. (21) is modified, as shown by AHNS, and becomes

$$c_3^2 = c_{30}^2 / \text{Re}(\epsilon). \quad (23)$$

Since the third-sound wavelengths are much longer than either the diffusion length or the sphere sizes that we consider, the screening factor ϵ is just that given by Eq. (17). The effect of the vortices is to change σ_s^0 in Eq. (21) to the renormalized value σ_s . AHNS also showed that the inverse of the quality factor Q of a third-sound resonance is given by

$$1/Q = 2\pi[\text{Im}(\epsilon)/\text{Re}(\epsilon)]. \quad (24)$$

This is the attenuation from vortex pairs, and we have again neglected the possible contribution from free vortices. Since $\text{Im}(\epsilon)$ increases at the KT transition, there will be a rapid drop in the Q as the transition is approached.

There is a final correction factor to Eq. (21) for our particular geometry of packed powders. This is the scattering correction n that accounts for the tortuous geometry through which the wave travels.⁴⁴⁻⁴⁷ n is the ratio of the velocity on a flat substrate to the velocity of the same film in the porous medium. Hence the final form for the experimentally observable third-sound velocity is

$$c_3^2 = \frac{1}{n^2} \frac{\rho_s^b}{\rho\epsilon} \frac{3\alpha(d - D_0)}{d^4}. \quad (25)$$

Figure 6 shows the third-sound velocity for the flat substrate and two different sphere sizes calculated from this equation. The sound velocities are plotted against film thickness for a fixed temperature, 1.37 K. The film thickness is given in atomic layers, and we take the usual definition 1 layer = 3.6 Å. Frequencies are obtained from $\omega = c_3 k$, with $k = 0.56 \text{ cm}^{-1}$ corresponding to the fundamental mode of our experimental resonator, and the index of refraction is chosen to be unity. The dashed lines again show the region where the assumption of low vortex density begins to break down. The dotted-dashed line shows the sharp drop to zero of the flat-substrate static theory. The broadening of the transition as the sphere size is reduced is clearly observable.

The results of the calculation of the third sound Q for the same parameters is also shown in Fig. 6. As the sphere size is reduced, the values of the Q 's in the transi-

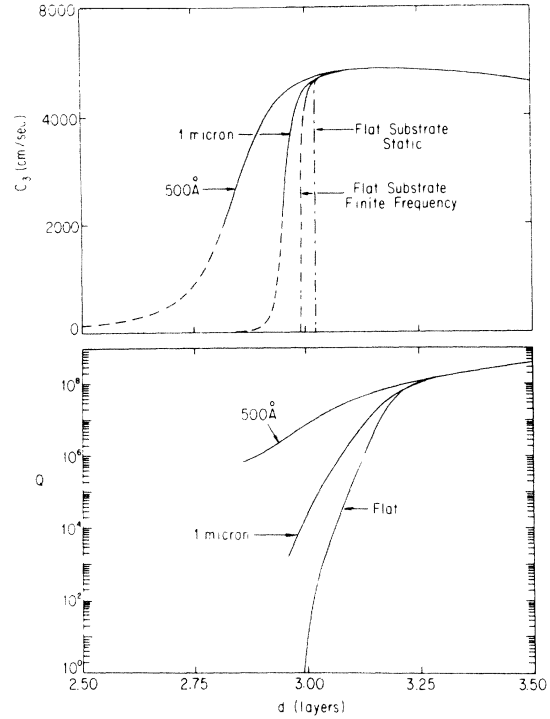


FIG. 6. Calculated third-sound velocity (upper curves) and Q factor (lower curves) for the different sphere diameters, at a temperature $T = 1.37$ K. The parameters are $E_c/K_0 = 2.2$, $a_0 = 20 \text{ \AA}$, and $D/a_0^2 = 2.5 \times 10^{10} \text{ sec}^{-1}$. The dashed lines show where $y > y_0$, and the dotted-dashed line shows the $\omega = 0$ flat-substrate result.

tion region increase greatly, corresponding to the same reduction of dissipation shown in Fig. 5. As in that figure, there is a change in Q near the onset region by about 3 orders of magnitude in going from the flat substrate to the 500-Å size. These plots show the attenuation from vortex pairs, and do not include other sources of third-sound attenuation such as coupling to the vapor or thermal losses to the substrate.⁴⁸ As discussed above for the torsion-oscillator dissipation, the calculation is not particularly valid for the region of high vortex densities, and the curves for the Q in Fig. 6 have been cut off near that point.

We have not justified the applicability of the simple sphere model to the actual experimental geometry. The packed powders are not isolated uniform spheres, but rather a collection of touching particles that are only crudely spherical. However, studies have shown that in these high-porosity systems the coordination number of particles touching a given particle is low, on the order of four or five.⁴⁹ We doubt that the vortex pairs on one sphere have much effect at all on pairs on a neighboring sphere. It is unlikely that the pairs can move freely from sphere to sphere through the narrow connecting bridges, although the hydrodynamics of such motion has not been studied. At low temperatures the dipole-flow cancellation of the relatively tightly bound pairs would result in very little interaction between pairs on neighboring spheres. In the transition region where σ_s approaches zero, however,

the average pair separation can approach the size of the sphere. In this regime there might be additional screening from "intervening" pairs on a neighboring sphere, although a quantitative estimate is quite difficult. Such screening would act to reduce the size of the tail of σ_s , in much the same manner as the high-vortex-density corrections.

The broadening of the superfluid density and the reduced dissipation predicted by the sphere model arise from the finite-length cutoff of the KT recursion. In the single-sphere case the cutoff length is clearly just the particle size. In the actual situation of touching spheres we believe that this will still hold true, since the particle size is the only "disorder" length in the system. The density of vortex pairs with separation greater than the sphere diameter may not drop identically to zero, but it is quite clear that there is a drastic limitation of the phase space for pairs of larger separation. In the next two sections we present data to show that this assumption gives quite reasonable agreement with experiments in packed powders.

III. APPARATUS AND PROCEDURE

A. Powder substrates

The substrates used in the present work are Al_2O_3 powders obtained from the Linde division of Union Carbide.⁵⁰ The three powder sizes used were Linde A (500 Å nominal diameter), Linde B (3000 Å), and Linde C (1 μm). After being packed in the resonator the porosity of each sample (the ratio of open volume to total volume) was measured by weighing, and the results were 0.75 for the 500-Å, 0.69 for the 3000-Å, and 0.70 for the 1- μm samples. The surface areas of the powders were estimated from N_2 -adsorption isotherms at 77 K, yielding 57 m^2/g for the 500-Å, 10 m^2/g for the 3000-Å, and 2.4 m^2/g for the 1- μm samples. Microphotographs of the 500-Å and 1- μm powders are shown in Ref. 45.

In the course of the sound-velocity measurements we also obtained the helium-adsorption isotherms for the three substrates in the temperature range 1.2–1.7 K. The isotherms for the 500-Å and 1- μm powders were virtually identical to those previously published.⁴⁵ In the thin-film regime the chemical potential for all three powder sizes varied accurately as $1/d^3$, the form expected if the films are uniform in thickness and the van der Waals force dominates. At higher thicknesses there is a deviation from this behavior due to the onset of capillary condensation.⁴⁵ This was most pronounced in the 500-Å powder because of its high radius of curvature, the deviation becoming noticeable just above four atomic layers. This is the reason that the sound-velocity data shown below in Fig. 12 departs from the van der Waals behavior in the region between four and five layers. Capillary condensation was observed in the 3000-Å and 1- μm powders at considerably thicker films, as expected, but we did find somewhat anomalous behavior for the 3000-Å powder. In this powder there were two distinct slope changes in the isotherm and sound-velocity data that showed capillary condensation occurring both at 4.6 layers and at 7.5 layers.

The origin of this anomaly was resolved when we noticed that the manufacturer's microphotograph⁵⁰ of the 3000-Å powder shows extensive surface roughness with a length scale of about 500 Å. The initial condensation is most likely on these surface features, and then the second capillary onset is from condensation between the particles. This behavior was not seen for the 500-Å or 1- μm powders, whose surfaces are known to be quite smooth.⁵¹

B. Experimental cell

The experimental cell used was an annular resonator similar to those used in earlier experiments on porous materials.^{44,45} A schematic of the cell is shown in Fig. 7. The powders were packed in an annular brass channel with a width of 1.1 cm and a mean circumference of 11.3 cm. Packing was done with a hydraulic press to pressures of about 3500–5000 psi. The powder was packed in 1-mm steps in order to keep the porosity uniform, and the final depths were about 10–12 mm. The final top surface was milled flat. The transducers were inset into a Plexiglass plate covering the top surface of the powder. Care was taken to have as flush as possible contact between the surface of the powders and the cover plate and transducers, to minimize any attenuation from coupling to sound modes in the vapor. The resonator assembly was sealed with an indium O-ring to a flange at the end of a cryostat probe, and placed in a standard 1-K Dewar system.

Several different drive and pickup methods were used in an attempt to obtain the best possible signals in the transition region. The different methods were used in the different powders, as the signals generally became smaller in the smaller powders. In the 1- μm powder cell the pickup used was an Allen-Bradley 200- Ω $\frac{1}{8}$ -W resistor with the case partially sanded to expose the carbon. The resistor was biased with a dc current of about 3 μA and at low temperatures had a resistance of about 100 $k\Omega$, resulting in power dissipation of less than 1 μW . In the 500-Å and 3000-Å powders the carbon resistor did not provide sufficient signals, so aluminum thin-film bolometers similar to the ones used in previous third-sound experiments were used.^{43,52} The strips had dimensions of 0.35×7.0 mm^2 , and a room-temperature resistance of about 600 Ω . The strips were evaporated onto a rectangular piece of glass

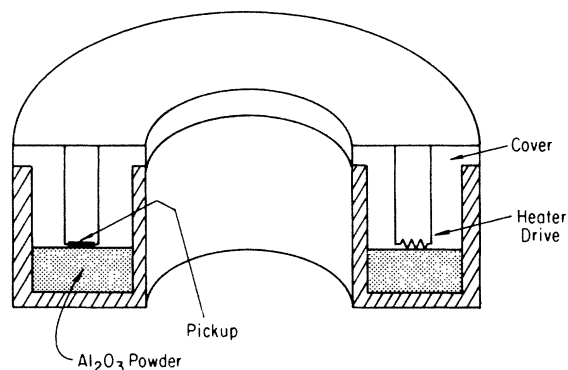


FIG. 7. Schematic of the cell, showing a cross section of the annular resonator.

which was then mounted in a groove in the top plate. A small dc current and magnetic fields were used to bias the bolometers on the superconducting transition, and this resulted in a typical power dissipation of about 5–10 μW .

The heater drive used in the 1- μm powder was a 50- Ω piece of resistance wire lightly epoxied to the top plate. In the 500- Å powder this type of drive did not produce sufficient signals in the transition region. However, good results were obtained by exciting the third-sound wave by lightly tapping on the Dewar. The free decay of the fundamental resonance is analyzed with a Unigon 113 fast-Fourier-transform (FFT) spectrum analyzer. Since this mechanical drive method gives no precise control over drive levels, it is arguable that the system could be driven nonlinearly in the higher-amplitude parts of the free decay. However, we did not observe any obvious changes from such effects in the course of the measurements on the 500- Å powder. The effects of high drive levels were studied in the two larger powders, and the results showed negligible shifts in the resonant frequency as a function of drive level. The measured sound velocities were also very reproducible from day to day, and we feel that the sound velocities obtained by this technique are quite accurate. In the 3000- Å powder mounting a heater wire on the top plate as in the 1- μm powder cell also did not provide sufficient signal. However, good results were obtained by packing the drive wire directly into the powder. Tapping on the Dewar was also tried in this powder, with no significant change in the results.

In the 3000- Å and 1- μm powder cells the drive frequency was swept using a Hewlett-Packard 2563 frequency synthesizer. Drive levels were kept as low as possible, on the order of 1–5 μW rms in the 1- μm powder and 5–20 μW in the 3000- Å powder. The output voltage of the pickups were amplified using a Princeton Applied Research 113 preamplifier and then analyzed with the FFT.

The ^4He film was built up by metering a known amount of gas into the cell, first passing it through a 77-K Zeolite cold trap. The film thickness d was determined by measuring the cell pressure p , and using the relation⁴⁵

$$\frac{R_g T}{M} \ln \left(\frac{p}{p_0} \right) = -\frac{\alpha}{d^3} + \frac{2\sigma}{\rho(R+d)}. \quad (26)$$

The left-hand side of this equation is the chemical potential of the gas, with R_g the gas constant, T the temperature, M the molecular weight, and p_0 the saturated vapor pressure. The right-hand side is the chemical potential of the surface of the film, and includes two contributions. The first term is the van der Waals energy, with d the film thickness and α the van der Waals constant, taken⁵³ to be 31 K (atomic layer)³. The second term is the surface energy, with σ the surface tension, ρ the liquid density, and R the sphere radius. This term has been included in the calculations of film thickness, although it is fairly small. The correction is largest in the 500- Å powder, where it ranged from 2% at 2.6 layers to 5% at 4.0 layers.

The cell pressure was determined by measuring the difference between the cell pressure and the bath pressure using a Baratron MKS 310BH-100 100-mm differential

pressure gauge with one end opened to the cell fill line and the other end opened to a tube inserted into the bath. The diameter of the fill line was 3 mm and, hence, the thermomolecular corrections to the pressure were negligible.

C. Procedure

Prior to an experimental run, the cell is pumped for at least 24 h. Noticeable water desorption can be observed for the first few hours. The cell is then flushed several times with ^4He gas before cooling to helium temperatures. Even after reaching the desired bath temperature, we found that additional precautions were needed to ensure that the powders reached the same temperature. The thermal conductivity of Al_2O_3 at low temperatures is very poor, and the normal He film is also a very poor conductor. The powder would not reach the bath temperature unless a superfluid film was present, and we used two methods to reach equilibrium. One was to build up the film thickness past the superfluid onset point, and then remove some of the liquid by warming the cell above 2 K and pumping the vapor away. The other method was to cool the cell well below the superfluid transition tempera-

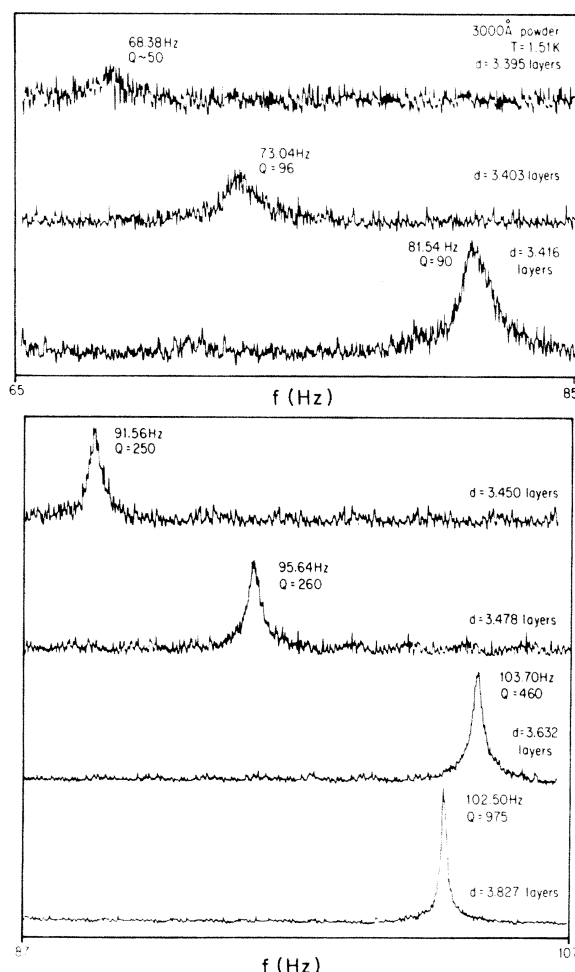


FIG. 8. Sample resonance curves in the transition region for increasing film thickness. Data are from the 3000- Å powder at 1.51 K.

ture, and then the warm back up to the desired temperature. As removing liquid from the film was a very time-consuming process, data was typically taken only as the film thickness was built up. In the onset region very small increments of gas were metered in, in thickness steps of ~ 0.01 layers. After each step several minutes were needed for equilibration, as monitored by the cell pressure.

Signals were very small in the onset region, and signal averaging of up to an hour per point was sometimes required. Several runs on successive days were generally needed to produce the data in the onset region, but the data were highly reproducible. Data from runs taken months apart showed deviations in sound velocity of less than the size of the symbols in the figures.

Figure 8 shows an example of the experimental spectra. This is for the 3000-Å powder at $T=1.51$ K, using the heater-wire drive. The resonance shown is the fundamental mode, where one wavelength fits into the mean circumference of the annulus. The first trace at the top is for a thickness of 3.395 layers, the thinnest film where any signal at all could be observed. In the second trace, only 0.008 layers thicker, there is a substantial improvement in the signal-to-noise ratio and in the Q , as well as an increase in the velocity. As the thickness is increased both the velocity and the Q continue to increase rapidly. At $d=3.63$ layers the velocity reaches a maximum (as σ_s levels off to a nearly constant value), and above this thickness the velocity begins to decrease due to the decreasing van der Waals force.

IV. RESULTS

A. Third-sound velocity

Figures 9–12 show the results for the third-sound velocity on a flat glass substrate and on the Al_2O_3 powders. As a reference point we have replotted in Fig. 9 the original flat-substrate data of Rudnick *et al.*⁵² in the region of the transition. The thickness scale of this plot has been corrected for the revised value of the van der Waals constant.⁴³ The hatched lines mark the superfluid onset

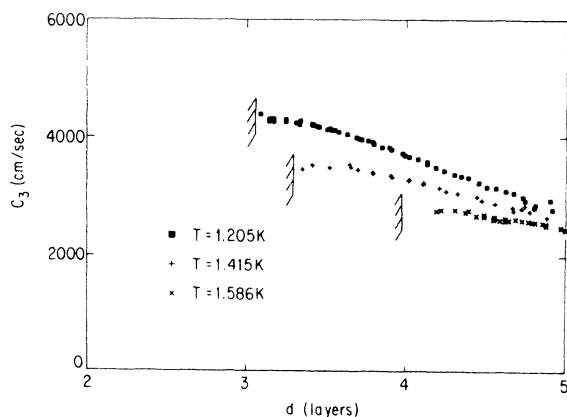


FIG. 9. Flat-substrate third-sound velocity in the onset region at three different temperatures. The data are taken from Ref. 51.

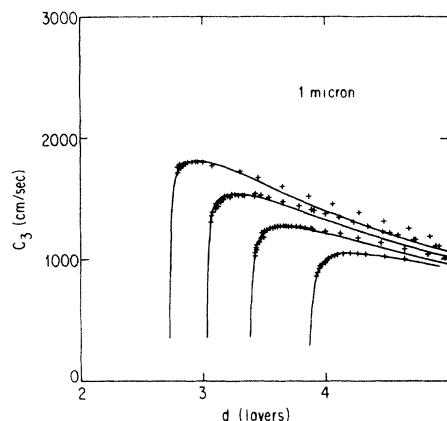


FIG. 10. Third-sound velocity vs film thickness in the 1- μm powder. The solid lines are fits to the sphere model, as discussed in the text. Temperatures are, from left to right, 1.21, 1.37, 1.51, and 1.62 K.

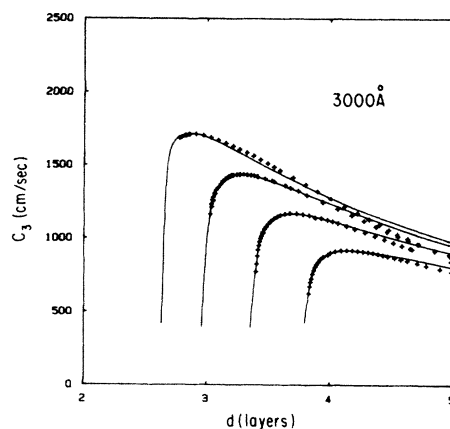


FIG. 11. Third-sound velocity vs film thickness in the 3000-Å powder. Temperatures are the same as for the 1- μm powder.

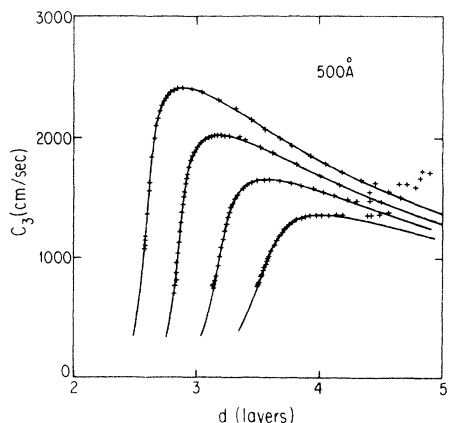


FIG. 12. Third-sound velocity vs film thickness in the 500-Å powder. Temperatures are the same as for the 1- μm powder.

points where the signal could no longer be observed due to a very rapid increase in attenuation. As discussed by Rudnick,¹⁵ the critical film thickness at which this occurs agrees very closely with the Kosterlitz-Thouless criterion of Eq. (15). The torsion-oscillator experiments of Bishop and Reppy¹⁷ showed that in fact σ_s drops rapidly to zero at these points. Both of these experiments served to confirm the KT vortex-screening picture of the superfluid transition in thin films.

Our results in the powders, Figs. 10–12, show behavior very similar to that seen in the flat-substrate data. As the film thickness is decreased the velocity rises from the increasing van der Waals force. A maximum value of c_3 is attained just prior to the drop in σ_s at the transition. By comparing Figs. 9 and 10–12, it can be seen that these maxima occur at the same thicknesses in all three powder sizes, and correspond very well to the critical thicknesses observed in the flat-substrate data. It is clear that the transition in the powders continues to occur at just the critical Kosterlitz-Thouless point. We conclude that, at least for powder grain sizes down to 500 Å, the vortex pairs still determine the nature of the transition.

On the other hand, there certainly are differences between the flat-substrate and powder results in the region of the transition. The decrease in σ_s becomes broadened and spread over a range of film thickness, and the degree of broadening increases as the powder grain size is decreased. There is also a decrease in the attenuation of the third sound, which allows the drop in σ_s to be observed, in contrast to the flat-substrate data. These characteristics of broadening and lowered attenuation are just those predicted by the finite-size Kosterlitz-Thouless model developed in Sec. II. The solid lines through the data points are theoretical fits to the sphere model, and this analysis will be discussed in more detail in Sec. IV C below.

The results for the 1- μm powder (Fig. 10) are the most similar to the flat-substrate results, but differences are observable even for this relatively large size. At thicknesses below the velocity maximum the beginnings of the drop in σ_s can be observed, but the signal is soon cut off by rapidly increasing attenuation. The 3000-Å data of Fig. 11 are fairly similar to those of 1 μm , but, in general, the signal could be observed over a larger portion of the onset region, as is most evident in the higher-temperature curves. The broadening of the drop in σ_s is most apparent in the 500-Å data of Fig. 12. Particularly at the higher temperatures the transition is seen to be quite smooth and continuous. The signal can be followed to very low values of σ_s , on the order of 10% of the value at the velocity maximum. As with the larger powders, however, the signal is finally again cut off by rising attenuation.

B. Attenuation

The attenuation of the third sound is characterized in terms of the quality factor of the resonance, $Q = f_0/\Delta f$, where Δf is the width of the resonance curve at the half-power points and f_0 is the resonant frequency. Figures 13–15 show the Q as a function of film thickness for the three powders at $T = 1.37$ K. The sound velocities are

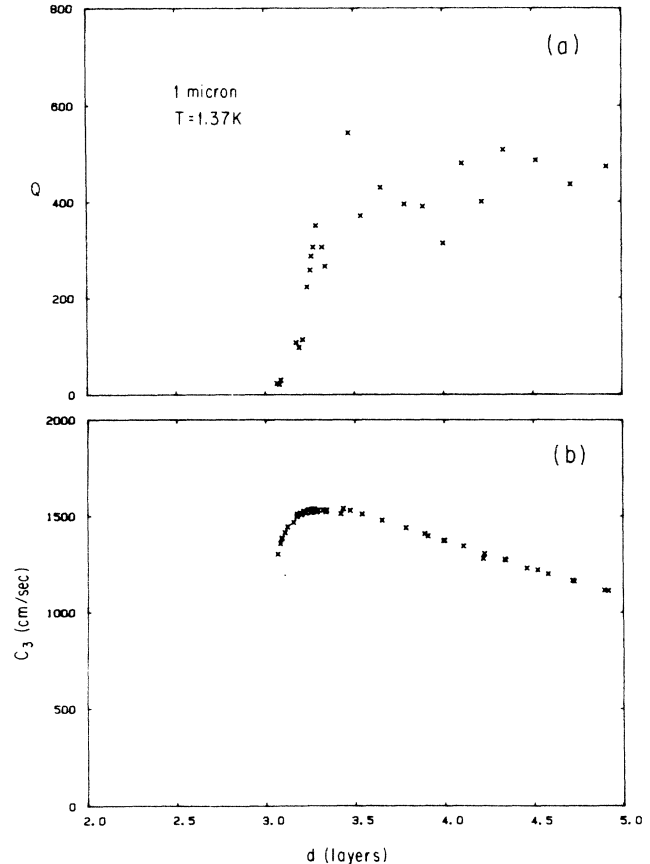


FIG. 13. (a) Third-sound attenuation and (b) velocity in the 1- μm powder at 1.37 K.

also plotted for comparison. The measurements of the Q are quite sensitive to noise and minor perturbations of the shape of the resonance, and the scatter seen in the data arises from these factors.

The same general features are seen in the attenuation in all of the powders: near the transition the Q drops rapidly as the film thickness is lowered, while for the thicker films it is nearly constant. The Q 's are highest in the 500-Å powder, and decrease appreciably in the larger powders. The signal can be observed in the 500-Å powder over a larger range of the drop in σ_s because of this lower attenuation. Even at the last observable point in the 500-Å data the Q is still about 50, and the third-sound mode remains well defined. In the larger powders the Q falls to small values much closer to the maximum in the sound velocity. This is similar to the flat-substrate data where third sound becomes diffusive very close to the maximum.⁵⁴

As mentioned in Sec. III, the effect of increasing the heater-drive level was studied for the 3000-Å and 1- μm powders.⁵⁵ Changes in the Q were the primary nonlinear effect observed, as there was very little shift in the resonant frequency even when the power was increased by 1 or 2 orders of magnitude. The effects on the Q were most pronounced in the 1- μm powder in the vicinity of the onset. At $d = 2.828$ layers and $T = 1.21$ K, increasing

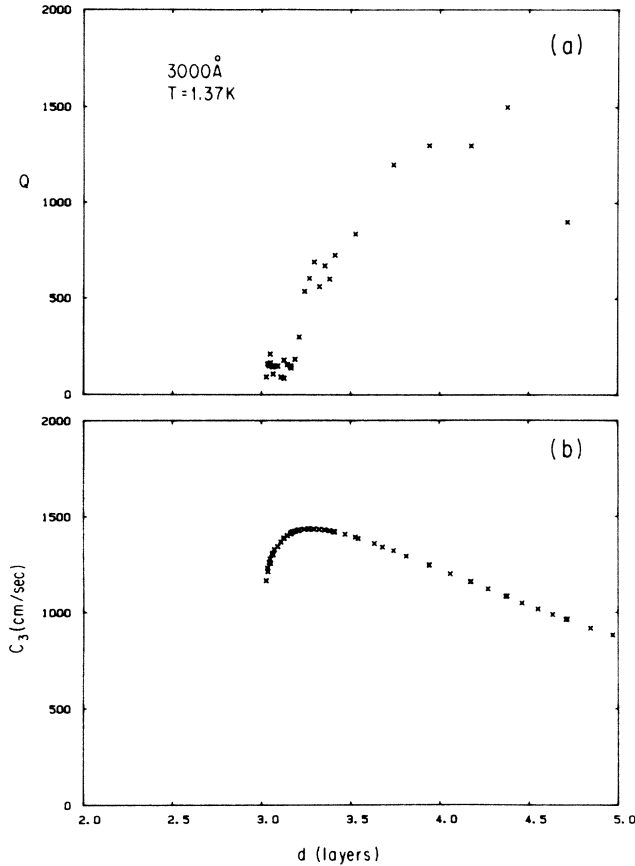


FIG. 14. (a) Third-sound attenuation and (b) velocity in the 3000-Å powder at 1.37 K.

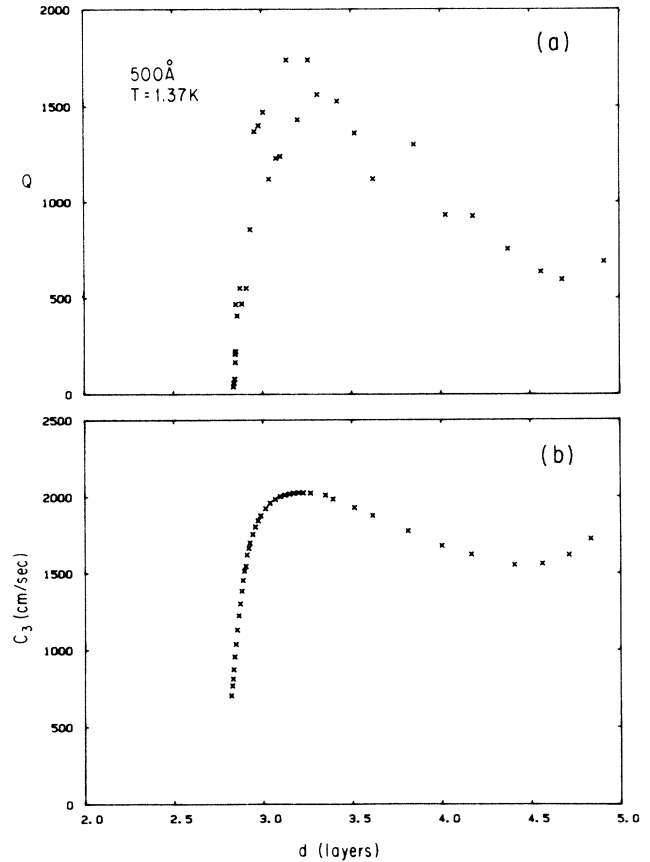


FIG. 15. (a) Third-sound attenuation and (b) velocity in the 500-Å powder at 1.37 K.

the drive level from 2 to 20 μW caused a decrease in the Q by a factor of 4, whereas the peak frequency changed less than 0.5%. For thicker films away from onset the Q change was much smaller, i.e., at $d = 4.03$ layers there was only a 20% decrease for the same power increase.

C. Comparison with sphere model

The sphere model developed in Sec. II predicts that limiting the maximum vortex-pair separation to the powder grain size will lead to a broadening of the transition and a reduction of the vortex dissipation as the powder size is decreased. The data presented above show at least qualitative agreement with this model. To attempt a more quantitative analysis of the third-sound velocity using Eq. (25) requires fitting four unknown parameters: The index of refraction n , the nonsuperfluid effective thickness D_0 , and the two vortex parameters E_c and a_0 needed for the computation of ϵ from Eq. (11). We assume that the sphere radius R is the nominal radius of the powder grains. In fitting to the data, the various parameters are sensitive to different regions of the experimental curves. n shifts the overall magnitude of the sound velocity, while D_0 shifts the film thickness at which the transition occurs. E_c primarily controls the rounding of the curves at the maximum in the sound velocity, and also plays a role in determining the onset thickness, shifting it to lower d if E_c is decreased. The core parameter a_0 determines the broadening of the transition region; larger

values of a_0/R broaden the thickness range over which σ_s drops to zero. There is a fair amount of correlation among the different parameters; for example, increasing a_0 or decreasing E_c to fit one region of the curve must be compensated by a decrease in D_0 to maintain the fit in other regions. The relatively large number of free parameters involved and the correlation between them unavoidably lessens the physical significance of the parameters resulting from the fits. However, the values obtained do correspond reasonably well to theoretical expectations.

For the 500- and 3000-Å powder data, the fits were performed allowing all four parameters to vary. The values of a_0 are very sensitive to the low-velocity data points in the onset region. Because of the lack of these points in the 3000-Å data, the values of a_0 are quite scattered and not terribly reliable, so a second set of fits were performed holding a_0 constant at the same values found in the 500-Å powder. The same problem is present in the 1- μm data, and the 500-Å values of a_0 were also used there. The parameters from the fits are shown in Table I, and the curves generated from the fits are shown as the solid lines in Figs. 10–12. For the 3000-Å fits the curve shown is for the parameters using the 500-Å values of a_0 , but the other set of parameters would make only a very slight visual difference in Fig. 11.

With the possible exception of a_0 , the resulting parameters are quite reasonable considering the simplicity of the

TABLE I. Parameters resulting from fits of the powder data to sphere model.

	T	a_0	E_c/K_0	D_0	n
500 Å	1.21	24	2.2	1.48	2.35
	1.37	23	2.3	1.60	2.40
	1.51	33	2.2	1.67	2.44
	1.62	50	2.1	1.81	2.42
1 μm	1.21	a	2.3	1.58	2.98
	1.37	a	2.2	1.65	3.01
	1.51	a	2.2	1.80	2.95
	1.62	a	2.2	2.06	2.80
3000 Å	1.21	18	a	1.56	3.29
	1.37	62	2.5	1.74	3.21
	1.51	52	2.5	1.93	3.22
	1.62	45	2.5	2.11	3.38
	1.21	a	1.6	1.13	3.55
	1.37	a	2.1	1.58	3.31
	1.51	a	2.1	1.75	3.31
	1.62	a	2.7	2.18	3.31

^aValues held constant at 500-Å values.

model used. The values of n are constant for each powder and range from about 2.4 to 3.3, and are similar to values found in previous experiments.^{45–47} The values of D_0 are smaller by a few tenths of an atomic layer than values obtained from earlier third-sound experiments,⁴³ and increase with increasing temperature. The values of E_c/K_0 are all fairly constant, about 2.2–2.5, and are relatively independent of temperature. The details of the core structure are not well understood, and several theoretical values of the core energy are available depending on the particular model of the core chosen. These values are $\pi/4 \simeq 0.8$ for a classical hard core in solid-body rotation,⁵⁶ 1.2 for an interacting Bose gas core,⁵⁶ and $\pi^2/2 \simeq 4.9$ for a 2D XY model vortex.¹⁰ Our experimentally obtained values are within the range of these numbers. There has also been a recent experimental determination of E_c/K_0 from flat-substrate third-sound measurements of Kono *et al.*⁵⁷ By fitting to the $\omega=0$ static theory in the onset region, they find $E_c/K_0 \simeq 7.8$, higher than the values listed above but not unreasonable. It is not entirely clear whether the static theory is a good approximation even at their lowest frequency of 3 kHz; as shown in Fig. 6 there is an appreciable difference in the “square-root cusp” region between $\omega=0$ and frequencies of even a few hundred Hz.

Our results for the vortex core radius are in the range of 20 to 50 Å, increasing with temperature. These values are significantly higher than would be expected for an isolated vortex in bulk liquid. Model calculations for bulk ^4He carried out by Glaberson⁵⁸ give values increasing from about 3 to 6 Å over our temperature range; an order of magnitude discrepancy. However, it is not apparent that the vortex core in a very thin film would be the same as in bulk. In the films the active superfluid layer is only one or two layers thick, and the vortex structure will be

strongly perturbed by the close proximity to the solid substrate and to the free surface. This could only act to increase the effective core radius. Another factor is that these are vortex pairs, and each core is distorted by the high flow field of its neighboring pair. The values of a_0 depend on the short-range behavior of the vortex interaction potential; Jones and Roberts³¹ have shown that this is appreciably modified by the distortion effects. The high values of a_0 could reflect modifications of the potential not accounted for in our simple model.

The fit parameters are certainly dependent on the particular idealized model that we have employed. The actual experimental geometry is undoubtedly more irregular and complex. The powder particles are not exactly spherical, and they are not completely isolated. There is also a distribution of grain sizes. An attempt to accommodate this last effect has been made by convoluting the calculation of σ_s over a Gaussian distribution of sphere sizes. This showed no appreciable change in the transition features. A skewed distribution would definitely affect the transition region, but there is no obvious necessity for the use of such a distribution.

Detailed fits to the attenuation data were not attempted because even rough quantitative agreement could not be found. The calculated values of the Q 's all tend to be orders of magnitude higher than the experimental values, as can easily be seen by comparing Figs. 13–15 with Fig. 6. The qualitative features are similar: a slowly changing Q at thick films and then a rapid drop in the onset region, with the smallest powder having the least attenuation because the grain size is so much smaller than the vortex diffusion length. The relative change in the theoretical Q between the flat substrate and 500 Å is roughly 3 orders of magnitude in the onset region; experimentally, the 500-Å Q is $\sim 10^3$ at a point where the flat-substrate data of Wang and Rudnick⁵⁴ would give a $Q \sim 1$.

The reason for the large numerical discrepancy between theory and experiment for the attenuation is not clear. The disagreement occurs not only with the powders, but also for the flat-substrate case. This suggests that the problem may not be specific to the adaption of the AHNS theory to a spherical surface, but are perhaps difficulties with the overall theory itself. Agnolet and Reppy have also observed features of the torsion-oscillator dissipation that cannot be explained by the AHNS theory.^{18,19} They find a many-orders-of-magnitude variation in the parameters resulting from the data fits, with values of D/a_0^2 ranging between 10^{11} and 10^{19} sec^{-1} .

A further problem in comparing third-sound attenuation with the theory is that there are additional sources of third-sound attenuation which are neglected in the calculation. These effects include coupling to the vapor above the film and thermal losses by substrate heat conduction. These have been studied both experimentally⁵⁹ and theoretically⁴⁸ for flat substrates, but a complete understanding is still lacking. The powder system is an even more complicated geometry for the evaluation of such effects. The uncertainty of the thickness and frequency dependence of this “background” attenuation make it difficult to separate the vortex attenuation from the other sources.

As mentioned in Sec. II the theoretical calculation also does not include contributions from “free” vortices, which might give an additional contribution to the attenuation and lower the discrepancy. This would be most important in the regime of high vortex densities, where $\gamma > \gamma_0$ and the dilute approximation for calculating the imaginary part of ϵ is becoming invalid.

V. DISCUSSION OF THE VYCOR DATA OF REPPY AND CO-WORKERS

The results presented above indicate that vortices remain the dominant mechanism in the superfluid transition of helium films adsorbed in powders of grain size down to 500 Å. This is in contrast to the conclusions reached by Reppy and co-workers from data on helium films in porous Vycor glass (Corning no. 7930). They postulated that the transition in that case was three dimensional,^{20–22,24,25} and that vortices played no role at all in the transition. As a result of our measurements, we have come to disagree with their conclusion, and in this section we discuss the Vycor data in more detail. We propose as an alternate hypothesis that the Vycor data are well described by a finite-size Kosterlitz-Thouless transition.

A. Superfluid density

Figure 16 shows a comparison of the torsion-oscillator data of Reppy and co-workers for films on flat substrates and on Vycor. Figure 16(a) is the Mylar substrate data of

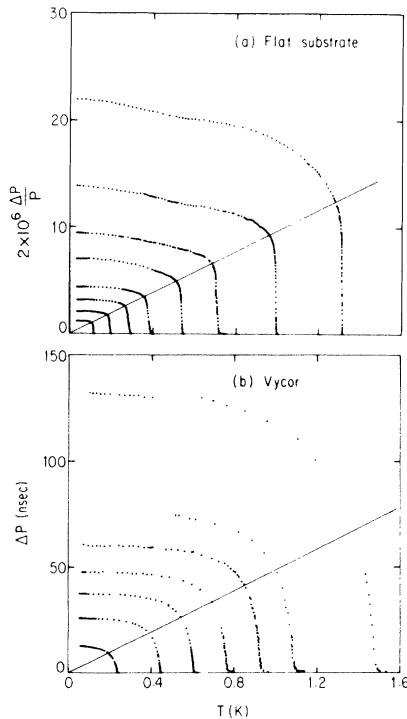


FIG. 16. Data of Reppy and co-workers for the torsion-oscillator period shift vs temperature for (a) the flat Mylar substrate (Refs. 18 and 19) and (b) for the Vycor (Refs. 20 and 21). The solid lines show the calibration of the KT “universal jump” point with slope given by Eq. (15), as discussed in the text. This figure should be compared with Fig. 4.

Agnolet,^{18,19} and Fig. 16(b) is the Vycor data of Bishop *et al.*^{20,21} The oscillator period shift ΔP is proportional to the superfluid mass, and the various curves represent different film thicknesses, thicker films having higher T_c 's. We point out the remarkable similarity of the data for the two substrates. In both cases the T_c increases linearly with increasing film thicknesses above the onset thickness. This is just the behavior expected for the Kosterlitz-Thouless transition, and in fact for both substrates the transition occurs at the critical KT point, as indicated by the straight solid line in both figures. These lines have a slope corresponding to the KT “jump” condition $\sigma_s/T = 3.5 \times 10^{-9}$ g/cm²K. The calibration of the jump line in terms of ΔP in Fig. 16(a) is given by Agnolet;¹⁹ we have added the line in Fig. 16(b) using the calibration data of Fig. 12 of Ref. 21. This calibration gives a sensitivity to superfluid mass of $\Delta P/m_s = 8.33 \times 10^3$ nsec/g, and multiplying by the measured area of the Vycor sample,⁶⁰ 170.6 m², gives $\Delta P/\sigma_s = 14.2$ sec cm²/g. Combining this with the above KT jump condition gives $\Delta P/T = 49.6$ nsec/K, and this is the slope of the line plotted in Fig. 16(b).

There are also clearly differences between the flat-substrate and Vycor curves of Fig. 16. The Vycor data show a broadening of the transition, a smooth decrease of the superfluid mass to zero rather than a sharp jump. We suggest that this broadening is due to a finite-size limitation of the KT transition, as discussed above. Our experimental data in the powders show just the same behavior: the drop in superfluid density begins at the KT onset point but then proceeds more slowly than the flat-substrate drop, with the degree of broadening increasing with decreasing grain size. Recent microphotographs⁶¹ of the Corning Vycor show that its structure is fairly similar to that of a packed powder, with grains of glass about 150 Å in diameter sintered together.⁶² (The mean pore size appears to be about half the diameter of the grains, i.e., ~ 75 Å, in agreement with previous estimates.⁶³)

The data of Fig. 16 are well described by the model of vortices on a sphere, shown in Fig. 4 for the 150-Å grain size. This figure uses the value of E_c found for the Al₂O₃ powders; more detailed fits of the model to the Vycor data yield somewhat larger core energies. For example, the curve in Fig. 16(b) with a $T_c = 0.45$ K yields best-fit values of $E_c/K_0 = 3.2$ and $a_0 = 11$ Å. As can be seen from comparing Figs. 4 and 16, the “tail” region of the model is considerably larger than the tail that is observed in the Vycor, and the data points in this region were excluded from the fits. As discussed for the dashed portion of Fig. 3, this is the region where the dilute approximation of the model is no longer valid.

B. Dissipation

The lack of observable dissipation at the transition was cited in Refs. 20–22, 24, and 25 as evidence that vortices are no longer involved and the system is three dimensional. As we have pointed out above, however, the finite-size limitation of the vortices leads to a rapid decrease in the dissipation peak as the grain size is reduced. Extrapolation of the dissipation calculation shown in Fig. 5 to the 150-Å size gives a peak value that is 4 orders of magni-

tude smaller than the flat-substrate peak. This would be extremely difficult to resolve in the torsion-oscillator experiments, particularly since the dissipation would be very broad and spread out compared to the sharp flat-substrate case.

As our powder measurements show, however, even small values of dissipation are observable in third-sound measurements, finally causing a loss of the signal. The difference is that in third sound all of the kinetic energy is in the helium film and is quite small, while for the torsion oscillators the kinetic energy is in the large oscillator mass, and the energy dissipation in the film is only a very tiny perturbation. In fact, the small dissipation in Vycor films has been observed in the third-sound measurements carried out by Bishop *et al.*²¹ The third-sound signal showed a smooth decrease of the superfluid density near the transition, but could not be carried to $\sigma_s = 0$ because “. . . the resonances become strongly damped and one cannot follow them. . . .”²¹ This behavior in the Vycor is very similar to our third-sound results in the 500-Å powder (Fig. 15).

C. Coherence length

In order for the helium films in Vycor to be characterized as three dimensional, it is necessary for the superfluid coherence length to be larger than the Vycor grain size at all temperatures. If the coherence length were only the 3–4 Å thought to characterize the bulk fluid and flat films, the Vycor films would necessarily have to be treated as two-dimensional systems (and hence subject to a Kosterlitz-Thouless transition).

Reppy²⁵ has advanced an argument that does lead to very long coherence lengths, although the argument is circular in nature. The coherence length is first *assumed* to be larger than the grain size. This leads to an unusual “coarse-grained” definition of the superfluid density,

$$\tilde{\rho}_s = \frac{m_s}{V_{\text{total}}}, \quad (27)$$

where m_s is the superfluid mass in the total Vycor volume, which includes the volume of the glass and the volume of the vapor spaces as well as the volume of the helium film. Since the glass and vapor volumes are very large compared to the helium volume, $\tilde{\rho}_s \ll \rho$ even at low temperatures. Using the expression for the coherence length,⁶⁴

$$\xi = \left[\frac{m}{2\pi\hbar} \right]^2 \frac{k_B T}{\tilde{\rho}_s}, \quad (28)$$

then gives values of ξ many hundreds of angstroms, since $\tilde{\rho}_s$ is so small, and this “confirms” the original assumption of a long coherence length.

We point out that an equally circular argument can be advanced to prove just the opposite result, that $\xi \sim 3\text{--}4$ Å, as in bulk helium. If we first assume that the coherence length is small compared to the grain size, then we must use the usual definition of the superfluid density,

$$\rho_s = m_s / V_{\text{He}}, \quad (29)$$

where now V_{He} is just the volume of the active superfluid portion of the film. At low temperatures this is known to be $\rho_s \sim \rho_s^{43}$ and inserting this value in Eq. (28) gives $\xi \sim 3\text{--}4$ Å, “confirming” the original assumption that the coherence length was small. There seems to be no *a priori* reason for choosing one of these two coherence length arguments over the other one.

D. Dilute 3D Bose gas

In the most recent series of measurements on the Vycor-film system, Crooker *et al.*²⁴ have extended the temperature range down to 3 mK, and at the lowest temperatures claim to see a crossover to the dilute limit, an ideal 3D Bose gas. For the ideal gas the superfluid mass should approach a linear dependence on $T - T_c$ at the transition. In the experiments the data for coverages with $T_c < 10$ mK do appear to have less curvature than the higher- T_c curves. This is a difficult region in which to take data because the superfluid mass is very small and thermal equilibrium becomes difficult. There is also a problem in subtracting the “tail” region, and this will be discussed below.

The experiments in the Vycor motivated theoretical work by Rasolt *et al.*⁶⁵ supporting the ideal Bose-gas picture. They developed a scaling function for the superfluid density to describe the evolution of the Bose transition as the fluid density is lowered and the system becomes dilute. When the low-temperature data ($T < 76$ mK) was plotted according to the scaling variables, the curves for different film thickness did collapse fairly well onto a single curve, in agreement with the theory.

We point out that the scaling of the Vycor data, although interesting, is not a definitive proof of the 3D Bose-gas model. As discussed above, the flat-substrate and Vycor curves in Fig. 16 are very similar. We find that applying the same scaling laws to the 2D flat-substrate data of Fig. 16(a) at the lowest temperatures also results in a collapse onto a single curve. Figure 17

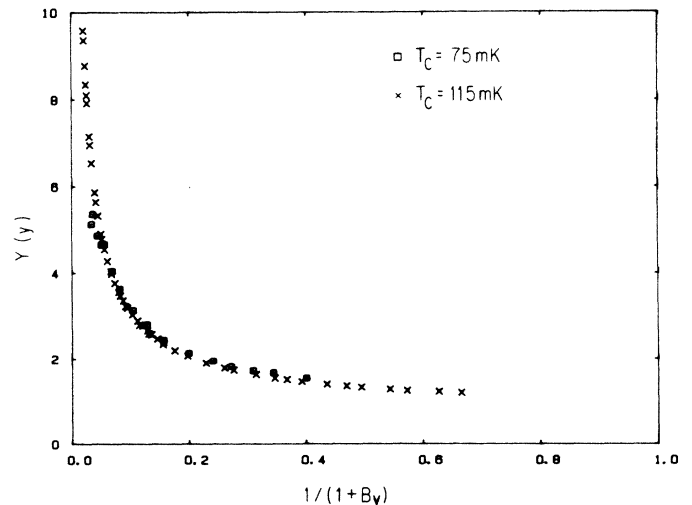


FIG. 17. Scaling plot of the two lowest-temperature flat-substrate curves of Fig. 16(a), the curves having T_c 's near 115 and 75 mK. The scaling is the same as that of Fig. 1 of Ref. 65, where the various parameters are defined.

shows the two lowest curves of Fig. 16(a) plotted using the same variables and parameters as the plot in Ref. 65. The flat-substrate data seem to scale in just the same manner as the Vycor results, although unfortunately the existing data do not extend to as low a temperature range. The scaling theory may well be perfectly correct, but it appears not to be a decisive test to differentiate between two-dimensional or three-dimensional behavior in the experiments.

The "tail" region of the Vycor data is a bothersome feature of the experiments. As can be seen in Fig. 1 of Crooker *et al.*,²⁴ the tail limits the region over which the "two-thirds" power law can be fitted. It also leads to problems in interpreting the very-lowest-temperature curves in this figure, which are claimed to be approaching the nearly linear dependence on $T - T_c$ of the ideal Bose gas. The size of the tail^{22,60} becomes comparable to the total superfluid signal for the curves with $T_c < 10$ mK, and it is unclear why the tail portion should not be subtracted in analyzing the data. The tail has opposite curvature to that of the "two-thirds" power law, and a combination of the two would tend to produce the more linear temperature dependence that is observed.

As discussed in Sec. II, on the other hand, the existence of the tail predicted by our sphere model is a natural consequence of the finite-size nature of the model. A very similar tail is also predicted by the flat-substrate AHNS theory. There the tail again results from the finite-size limitation on the maximum separation of the vortices, to distances less than the diffusion length r_D . These tails are clearly observed in the flat-substrate torsion-oscillator measurements of Reppy and co-workers,^{17,19} in agreement with the AHNS theory. The existence of the same type of tails in the Vycor measurements is not at all surprising from the viewpoint of a finite-size KT model.

A final question with the Bose-gas interpretation is whether the helium ever really becomes dilute. In the view of Reppy and co-workers, the nonsuperfluid portion of the film closest to the substrate is taken to be rigidly frozen solid, with individual "superfluid" atoms skating freely above.^{20-22,24,25} At the lowest coverages the spacing between the superfluid atoms is deduced²⁵ from this model to be on the order of ~ 100 Å, and hence the claim that the system is dilute.

In fact, every helium atom in this system is never separated by more than 3.6 Å from another helium atom, and the degree of diluteness depends on the conjectures made about the "dead" layers of helium. The measurements of superfluid mass only prove that these layers are *not superfluid*, and do not imply that they are completely frozen solid. Some fraction could well be liquidlike, but *normal* liquid. It is very well known that solid helium is the least solidlike of any material⁶⁶ and has many similarities to the liquid state. There is some experimental evidence that the nonsuperfluid layers are really not completely inert. Measurements on spin dynamics of adsorbed ³He layers⁶⁷ show that there is a rapid interchange of atoms between the first and second adsorbed layers. Torsion-oscillator measurements on ⁴He films show an unexpected temperature-dependent signal arising from these layers, prior to the onset of superfluidity.¹⁹ It is also

well known that above 1 K the nonsuperfluid thickness D_0 increases with temperature,⁴³ and certainly contains a large fraction of normal liquid. If even a small portion of the adsorbed layers on Vycor are normal fluid at low temperatures, it would be meaningless to try to identify individual superfluid atoms, just as in bulk helium. In this case the system could not be characterized as dilute at all.

VI. CONCLUSION AND DISCUSSION

The results presented above in Secs. II–IV provide a coherent picture of the superfluid transition of helium films in porous materials. The KT vortex transition on flat substrates evolves continuously as the grain size is reduced, with the grain size being the natural cutoff length for the maximal vortex pair separation. This leads to a finite-size broadening of the transition and a sharp reduction of the vortex dissipation for grain sizes smaller than the vortex diffusion length. The third-sound measurements in Al₂O₃ powders show just this type of evolution from the flat-substrate results, and the Vycor data of Fig. 16 are also quite consistent with this picture.

Because of the importance of understanding the nature of the superfluid transition, further experimental work is certainly necessary to clarify the mechanism involved. The powder measurements need to be extended to a wider range of grain sizes. Carbon-black powders may be suitable for this purpose, since fairly uniform powders can be obtained having grain sizes down to ~ 100 Å. The measurements also need to be carried out at considerably lower temperatures in order to allow a more direct comparison with the Vycor measurements of Reppy and co-workers. Below 1 K the temperature can be varied at fixed film thickness, which could not be done in the present experiments because of thinning from evaporation. We also suggest torsion-oscillator measurements using the packed-powder substrates. Our model gives rather clear predictions (Fig. 5) for the trend of the data as the powder size is reduced. The oscillators would be particularly useful for the dissipation studies since they are able to track the signal completely through the transition.

A question which our results bring up is how the superfluid transition evolves as further liquid is added to the films in the packed powders, enough to completely fill the pores. The thermally fluctuating vortex pairs responsible for the transition in films will certainly still be present. Instead of terminating at the free surface they will extend to the opposing powder grain or (near the center of a pore) loop together to form rings. It is a matter of speculation as to whether these vortex pairs would act to reduce the superfluid density to zero as the temperature is increased, in much the same manner as with the films. The maximal pair separation will presumably be limited by the pore size, leading to finite-size effects. Experiments in fine packed powders⁶⁸ do observe finite-size tails in the superfluid density, similar to those discussed in the sections above.

Even more speculative is the question of whether such vortices would continue to play a role as the pore size is increased toward the bulk limit. In this case vortex rings of increasing size would be the equivalent of the vortex

pairs of the 2D KT theory. A central feature of the high-temperature and ϵ expansions describing the superfluid transition is the existence of fluctuations of the order parameter on long length scales as the transition is approached; fluctuating vortex rings of large diameter could well give rise to just such behavior. The most recent proposals that the λ transition might involve vortices have come from field theory,⁴ where studies of lattice gauge theories have led to an increasing understanding of the role of topological excitations in phase transitions.⁶⁹ It would be interesting if the original intuitive speculations of Onsager¹ and Feynman² could be shown to be equivalent to the more modern theories of the superfluid transition.

ACKNOWLEDGMENTS

We would like to acknowledge useful discussions with, among others, G. Agnolet, S. Baker, S. Hannahs, S. Putterman, J. Reppy, P. Roberts, J. Rudnick, and I. Rudnick. We also thank G. Agnolet and J. Reppy for providing the data used in Fig. 16. This work was supported in part by grants from the National Science Foundation, Nos. DMR-81-00218 and DMR-84-15705. One of us (G.A.W.) would also like to acknowledge support from the UCLA College Institute.

*Present address: Physics Dept., Texas A&M University, College Station, Texas 77843.

¹L. Onsager, *Nuovo Cimento Suppl.* **6**, 249 (1949).

²R. P. Feynman, in *Progress in Low Temperature Physics*, edited by C. J. Gorter (North-Holland, Amsterdam, 1955), Vol. 1, p. 17.

³Early papers include E. Byckling, *Ann. Phys. (N.Y.)* **32**, 367 (1965); V. N. Popov, *Zh. Eksp. Teor. Fiz.* **64**, 672 (1973) [*Sov. Phys.—JETP* **37**, 341 (1973)]; C. J. Morgan, H. W. Jackson, and S. A. Werner, *Phys. Rev. B* **18**, 2145 (1978).

⁴Field theory approaches include M. Peskin, *Ann. Phys. (N.Y.)* **113**, 122 (1978); R. Savit, *Rev. Mod. Phys.* **52**, 453 (1980); *Phys. Rev. B* **17**, 1340 (1978); H. Kleinert, *Phys. Lett.* **93A**, 86 (1982).

⁵Approaches from liquid-crystal theory include W. Helfrich, *J. Phys. (Paris)* **39**, 1199 (1978); D. R. Nelson and J. Toner, *Phys. Rev. B* **24**, 363 (1981); C. Dasgupta and B. I. Halperin, *Phys. Rev. Lett.* **47**, 1556 (1981); C. Dasgupta, *Phys. Rev. B* **27**, 1262 (1983).

⁶R. G. Bowers and G. S. Joyce, *Phys. Rev. Lett.* **19**, 630 (1967); M. Ferer, M. A. Moore, and M. Wortis, *Phys. Rev. B* **8**, 5205 (1973).

⁷J. C. LeGuillou and J. Zinn-Justin, *Phys. Rev. B* **21**, 3976 (1980).

⁸G. Ahlers, *Rev. Mod. Phys.* **52**, 489 (1980); P. Hohenberg, *Physica* **109&110B**, 1436 (1982).

⁹W. Helfrich (Ref. 5) has tentatively identified vortex loop contributions in a high-temperature expansion of the spin- $\frac{1}{2}$ XY model.

¹⁰J. M. Kosterlitz and D. J. Thouless, *J. Phys. C* **6**, 1131 (1973); J. M. Kosterlitz, *ibid.* **1046** (1974).

¹¹A. P. Young, *J. Phys. C* **11**, L453 (1979); *Phys. Rev. B* **19**, 1855 (1979).

¹²D. R. Nelson and J. M. Kosterlitz, *Phys. Rev. Lett.* **39**, 1201 (1977).

¹³M. E. Fisher, M. N. Barber, and D. Jasnow, *Phys. Rev. A* **8**, 1111 (1973).

¹⁴J. E. Van Himbergen and S. Chakravarty, *Phys. Rev. B* **23**, 359 (1981); J. E. Van Himbergen, *ibid.* **25**, 5977 (1982).

¹⁵I. Rudnick, *Phys. Rev. Lett.* **40**, 1454 (1978).

¹⁶E. Webster, G. Webster, and M. Chester, *Phys. Rev. Lett.* **42**, 243 (1979).

¹⁷D. J. Bishop and J. D. Reppy, *Phys. Rev. Lett.* **40**, 1727 (1978); *Phys. Rev. B* **22**, 5171 (1980).

¹⁸D. McQueeney, G. Agnolet, and J. D. Reppy, *Phys. Rev. Lett.* **52**, 1325 (1984).

¹⁹G. Agnolet, Ph.D. thesis, Cornell University, 1983 (unpublished).

²⁰J. E. Berthold, D. J. Bishop, and J. D. Reppy, *Phys. Rev. Lett.* **39**, 348 (1977).

²¹D. J. Bishop, J. E. Berthold, J. M. Parpia, and J. D. Reppy, *Phys. Rev. B* **24**, 5047 (1981).

²²E. N. Smith, D. J. Bishop, J. E. Berthold, and J. D. Reppy, *J. Phys. (Paris Colloq. C-6)*, 342 (1978).

²³A "two-thirds" power law has also been observed in porous materials when the pores are completely filled with helium: M. Kriss and I. Rudnick, *J. Low Temp. Phys.* **3**, 339 (1970); C. W. Kiewit, H. E. Hall, and J. D. Reppy, *Phys. Rev. Lett.* **35**, 1286 (1975).

²⁴B. C. Crooker, B. Hebral, E. N. Smith, Y. Takano, and J. D. Reppy, *Phys. Rev. Lett.* **51**, 666 (1983).

²⁵J. D. Reppy, *Physica* **126B+C**, 335 (1984).

²⁶V. Kotsubo and G. A. Williams, *Phys. Rev. B* **28**, 440 (1983).

²⁷V. Kotsubo and G. A. Williams, *Phys. Rev. Lett.* **53**, 691 (1984).

²⁸V. Kotsubo and G. A. Williams, in *Proceedings of the 17th International Conference on Low Temperature Physics*, edited by U. Eckern, A. Schmid, W. Weber, and H. Wühl (North-Holland, Amsterdam, 1984), Vol. 2, pp. 951 and 971.

²⁹V. A. Bogomolov, *Fluid Dynamics* **12**, 863 (1978).

³⁰S. J. Putterman, *Superfluid Hydrodynamics* (North-Holland, Amsterdam, 1974), p. 114.

³¹C. A. Jones and P. H. Roberts, *J. Phys. A*, **15**, 2599 (1982).

³²The commonly used form $\ln(r/a_0)$ is only an approximation to the vortex pair interaction, as noted in Ref. 10 and many textbooks on hydrodynamics. The form $\ln[(r-a_0)/a_0]$ is probably a better approximation at small r . The flat-substrate KT transition is not affected much by the difference between the two forms, since it mainly depends on the range $r \rightarrow \infty$ there they become identical.

³³J. L. Cardy and N. Parga, *J. Phys. C* **13**, 571 (1980).

³⁴J. Tobochnik and G. V. Chester, *Phys. Rev. B* **20**, 3761 (1979).

³⁵A. T. Fiory, A. F. Hebard, and W. I. Glaberson, *Phys. Rev. B* **28**, 5075 (1983).

³⁶K. Y. Szeto and G. Dresselhaus, *Phys. Rev. B* **32**, 3142 (1985).

³⁷K. Y. Szeto, S. T. Chen, and G. Dresselhaus, *Phys. Rev. B* **32**, 4628 (1985).

³⁸V. Ambegaokar, B. I. Halperin, D. R. Nelson, and E. D. Siggia, *Phys. Rev. B* **21**, 1806 (1980).

³⁹C. Wang and L. Yu, *Phys. Rev. B* **33**, 599 (1986). The numerical discrepancy with our calculation of σ_s , cited by these authors arises from their mistaken assumption that the labels of

- the curves in Fig. 2 refer to the radius of the sphere instead of the diameter. When this correction is made the two (rather different) calculations agree completely.
- ⁴⁰We take D to be a constant, although recent measurements by M. Kim and W. I. Glaberson [Phys. Rev. Lett. **52**, 53 (1985)] indicate that it may be a function of σ , over some portion of the transition region.
- ⁴¹G. B. Hess and R. J. Muirhead, J. Low Temp. Phys. **49**, 481 (1982); J. Maps and R. B. Hallock, Phys. Rev. Lett. **47**, 1533 (1981); R. A. Joseph and F. M. Gasparini, Physica **109&110B**, 2102 (1982); G. Agnolet, S. L. Teitel, and J. D. Reppy, Phys. Rev. Lett. **47**, 1537 (1981).
- ⁴²K. R. Atkins and I. Rudnick, in *Progress in Low Temperature Physics*, edited by C. J. Gorter (North-Holland, Amsterdam, 1970), Vol. 6, p. 37.
- ⁴³J. H. Scholtz, E. O. Maclean, and I. Rudnick, Phys. Rev. Lett. **32**, 147 (1974).
- ⁴⁴G. A. Williams, R. Rosenbaum, and I. Rudnick, Phys. Rev. Lett. **42**, 1282 (1979).
- ⁴⁵R. Rosenbaum, G. A. Williams, D. Heckerman, J. Marcus, D. Scholler, J. Maynard, and I. Rudnick, J. Low Temp. Phys. **37**, 663 (1979).
- ⁴⁶S. Baker, J. Marcus, G. A. Williams, and I. Rudnick, in *Physics and Chemistry of Porous Media*, edited by D. L. Johnson and P. N. Sen (AIP, New York, 1985), p. 119.
- ⁴⁷J. M. Valles, Jr., D. T. Smith, and R. B. Hallock, Phys. Rev. Lett. **54**, 1528 (1985).
- ⁴⁸D. J. Bergman, Phys. Rev. **388**, 370 (1969); Phys. Rev. A **3**, 2058 (1971).
- ⁴⁹W. Wade, J. Phys. Chem. **69**, 322 (1965).
- ⁵⁰Alumina Powder Information Brochure, Form CP 1/10, Linde Division of Union Carbide, Indianapolis, IN.
- ⁵¹D. L. Johnson and P. N. Sen, Phys. Rev. B **24**, 2486 (1981).
- ⁵²I. Rudnick, R. S. Kagiwada, J. C. Fraser, and E. Guyon, Phys. Rev. Lett. **20**, 430 (1968).
- ⁵³E. S. Sabisky and C. H. Anderson, Phys. Rev. A **7**, 790 (1973).
- ⁵⁴T. G. Wang and I. Rudnick, J. Low Temp. Phys. **9**, 425 (1972).
- ⁵⁵V. Kotsubo, Ph.D. thesis, University of California, Los Angeles, 1985 (unpublished).
- ⁵⁶R. J. Donnelly and P. H. Roberts, Proc. R. Soc. London, Ser. A **321**, 519 (1969).
- ⁵⁷K. Kono, S. Kobayashi, and W. Sasaki, J. Low Temp. Phys. **57**, 319 (1984).
- ⁵⁸W. I. Glaberson, J. Low Temp. Phys. **1**, 289 (1967).
- ⁵⁹J. E. Rutledge and J. M. Mochel, Phys. Rev. B **20**, 2659 (1984).
- ⁶⁰D. J. Bishop, Ph.D. thesis, Cornell University, 1978 (unpublished).
- ⁶¹K. Kadokura, Ph.D. thesis, University of California, Los Angeles, 1984 (unpublished). Microphotographs taken by Y. Bando at Arizona State University.
- ⁶²An analysis by P. Gammel of synchrotron radiation scattered from Vycor also leads to a grain size estimate of 150 Å: J. Reppy (private communication).
- ⁶³D. F. Brewer and D. C. Champeney, Proc. Phys. Soc. London **79**, 855 (1962).
- ⁶⁴R. A. Ferrell, N. Menyhard, H. Schmidt, F. Schwabel, and P. Szépfalussy, Ann. Phys. (N.Y.) **47**, 565 (1968); B. I. Halperin and P. C. Hohenberg, Phys. Rev. **177**, 952 (1969).
- ⁶⁵M. Rasolt, M. J. Stephen, M. E. Fisher, and P. B. Weichman, Phys. Rev. Lett. **53**, 798 (1984); P. B. Weichman, M. Rasolt, M. E. Fisher, M. J. Stephen, Phys. Rev. B **33**, 4632 (1986).
- ⁶⁶A. F. Andreev, in *Progress in Low Temperature Physics*, edited by D. F. Brewer (North-Holland, Amsterdam, 1982), Vol. 7, p. 67.
- ⁶⁷R. C. Richardson, Physica **126B+C**, 298 (1984).
- ⁶⁸I. Rudnick, E. Guyon, K. A. Shapiro, and S. A. Scott, Phys. Rev. Lett. **19**, 488 (1967).
- ⁶⁹J. B. Kogut, Rev. Mod. Phys. **51**, 659 (1979); **55**, 775 (1983).

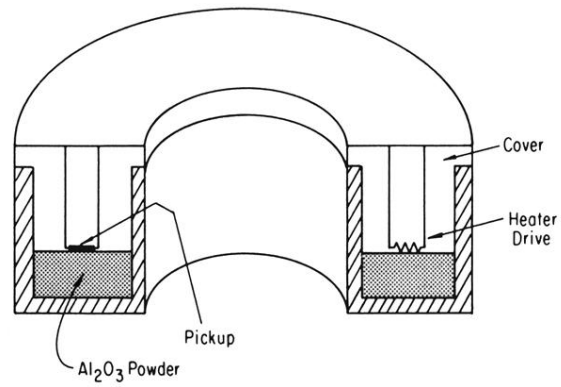


FIG. 7. Schematic of the cell, showing a cross section of the annular resonator.